Progress In Electromagnetics Research, Vol. 121, 89–101, 2011

INTEGRATED WAVEGUIDE STRUCTURE FOR HIGHLY SENSITIVE THZ SPECTROSCOPY OF NANO-LITER LIQUIDS IN CAPILLARY TUBES

V. Matvejev [1, *], C. de Tandt [1], W. Ranson [1], J. Stiens [1], R. Vounckx [1], and D. Mangelings [2]

[1]Laboratory of Micro- and Photoelectronics, LAMI-ETRO, Vrije Universiteit Brussel (VUB), Pleinlaan 2, Brussels 1050, Belgium

[2]Department of Analytical Chemistry and Pharmaceutical Technology, Vrije Universiteit Brussel (VUB), Laarbeeklaan 103, Brussels 1090, Belgium

Abstract—Terahertz dielectric spectroscopy permits the study of biomolecular interactions. However, water induces high attenuation of electromagnetic waves in the THz frequency range, obscuring the response of biomolecules. The developed sensor overcomes this problem by concentrating the THz wave propagating in an integrated waveguide on a small liquid volume contained within a capillary tube. Detailed electromagnetic modeling shows effective interaction between the THz waves and liquids. Transmission measurement results for capillary tubes filled with water and methanol mixtures demonstrate a substantial increase in sensitivity to changes of liquid permittivity. The current integrated sensor facilitates THz spectroscopy of biological liquids: a case study on buffered human serum albumin solution demonstrates a great potential to complement biochemical analytical tools.

1. INTRODUCTION

Numerous research publications prove that THz (10^{11}–10^{13} Hz) waves can probe various inter- and intra-macromolecular functional properties: biomolecule's [1–3] and lipid membrane's [4, 5] hydration, binding reactions with other biomolecules [6], conformational changes [7, 8] and its functioning [9]. This creates new possibilities for real-time, label-free biosensing of biomolecular entities of differing

Received 1 September 2011, Accepted 10 October 2011, Scheduled 15 October 2011

* Corresponding author: Vladimir Matvejev (vmatveje@etro.vub.ac.be).

complexity: cells, nucleic acids, proteins, polypeptides, carbohydrates, lipids.

The majority of studies were carried out with specially treated samples in order to overcome the severe attenuation of THz waves by liquids which shadows the biomolecules' response. Pressed pellets [10], hydrated films [11, 12] and cryogenically frozen samples enable free-space measurements to be carried out on biological samples with a reasonable sensitivity at THz frequencies. A disadvantage of these measurement methods is that the unnatural environment, does not allow investigations of biomolecule's conformational evolution with biological function. Another major drawback with free-space measurements is the necessity for large sample quantities and high-performance equipment (bright sources, sensitive detectors), which prohibits wide-scale application and commercialization.

Integrated THz sensing approaches have proved to be more sensitive and sample quantity-reducing [13], but measurements with sufficient hydration still present a challenge. In integrated sensors based on planar transmission lines [14, 15] the sample cannot be loaded at the location of maximum EM-field strength, resulting in a large propagation attenuation along the longer transmission line required for a longer interaction path length. In the case of a single wire transmission line the interaction is much stronger [16]. Both planar transmission lines and single wire transmission lines suffer from excessive losses which reduce the measurement sensitivity to dielectric permittivity changes in the sample [17–19].

This paper introduces a technique for highly sensitive THz liquid spectroscopy, which is suitable for bio-sensing applications. The integrated low-loss hexagonal cross-section waveguide (WH) [20] and commercially available fused silica capillary tube (CT) constitute an improved measurement technique. Sensor configurations with two CTs are tested and compared. Water and methanol measurements and simulations establish the high sensitivity of the proposed configuration. The methanol was selected as a well characterized simple organic polar liquid for sensor demonstration purposes and simulation-to-measurement comparisons for different sensor configurations. Numerical modeling results for a case study of buffered solution of human serum albumin in its natural and unfolded conformational states are presented.

2. SENSOR AND MEASUREMENT SETUP

The WH produced by bulk wet anisotropic etching is used as a basis for the sensor structure, where additional holes in the center

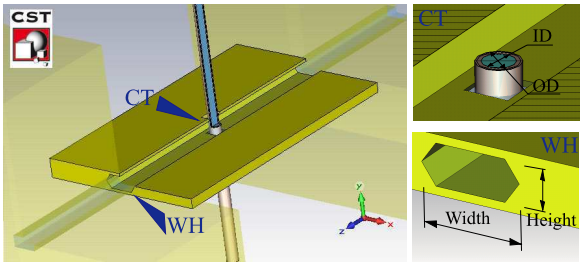

Figure 1. A cut away view of the WH-CT sensor configuration and expanded views of the CT and WH cross-sections with their dimensions.

of the WH were micromachined to allow insertion of a CT. The sensor was designed to operate in the 226–336 GHz band (WR3.4). The width, height and length of the WH were 1200 µm, 500 µm and 10 mm, respectively (see Figure 1). Several types of WH-CT sensor configurations were produced:

- WHCT100 — WH in combination with CT, $ID = 100\,\mu\text{m}$ and $OD = 360\,\mu\text{m}$
- WHCT320 — WH in combination with CT, $ID = 320\,\mu\text{m}$ and $OD = 435\,\mu\text{m}$

where ID is the inner and OD — the outer diameter.

The sensor configuration model with a quarter of it cut out along the WH is shown in Figure 1. Flanges are modeled by two brass ($\sigma = 2.47 \times 10^7\,\text{S/m}$) blocks (10 mm × 10 mm × 5 mm) with a WR-6.5 waveguide inserted in the center. The flanges are 10 mm apart. Between the flanges a chip with WH waveguide is placed. The chip is a gold ($\sigma = 4.09 \times 10^7\,\text{S/m}$) block with a thickness of 700 µm (twice the wafer thickness), a width of 6 mm and a length of 10 mm. The WH is modeled as a hexagonal prism cut out of the chip and filled with air. The hexagonal waveguide dimensions are 1200 µm × 500 µm × 10 mm. CT and liquids are modeled as three concentric cylinders: an inner cylinder with dielectric properties of the liquid has diameter ID (100 µm or 320 µm); a silica (CST material library: $\epsilon_r = 3.81$, $\tan\delta = 5 \times 10^{-4}$ at 281 GHz) tube with inner diameter — ID and outer diameter OD — 18 µm (OD is 363 µm or 435 µm); the polyvinyl (CST material library: $\epsilon_r = 3.49$, $\tan\delta = 1.9 \times 10^8$ at 281 GHz) coating of the CT is modeled by outer cylinder with outer diameter OD and inner diameter OD — 18 µm. The CT extends through the entire model. The ports (1 and 2) are defined on the end facets of dielectric corresponding to WR-6.5 enclosed in the metal of the flanges.

The open boundary (or Perfectly Matched Layer) boundary conditions are applied, absorbing all inward traveling waves. Only a quarter of the model is simulated (meshed), as simplification is permitted due two symmetry planes: magnetic ($H_t = 0$) on YZ-plane and electric ($E_t = 0$) on XZ-plane. The following meshing statistics have been applied: minimum mesh step 6.75 µm, maximum mesh step 60.14 µm and a total of 6.2×10^6 mesh cells. The water and methanol dielectric permittivity parameters for the 2nd order Debye model are taken from [21]. The 3D EM modeling is carried out with *CST Microwave Studio's* time domain solver, the Gaussian pulse is chosen as the port 1 time input signal for the Finite Integration Technique.

Since the chip with WH was not provided with flanges, the placement and alignment with the conventional flanges of the measurement equipment is carried out using an $XYZ\theta$ micro-translation stage. The measurements are performed with a Millimeter Vector Network Analyzer (MVNA) from AB Millimeter and WR-3.4 band front end components (see Figure 2). WR-to-WH coupling mismatch de-embedding is not attempted due to the poor reproducibility of reconnection using the micro-translation stage. This issue will be solved in the near future.

The chip loading procedure and liquid injection into the CT is done as follows. First, the measurement equipment is calibrated up to the front end output flanges. Then the chip with WH is aligned in the proximity of the reflection and transmission measurement arm flanges, the chip is pressed into contact and fixed by the movable transmission arm, and finally the CT is vertically inserted and one end is attached to a syringe suspended above the WH chip. The syringe is refilled by removing the plunger, so that the syringe barrel and the CT remain all the time in their initial positions. A picture of the assembled measurement system is shown in Figure 2.

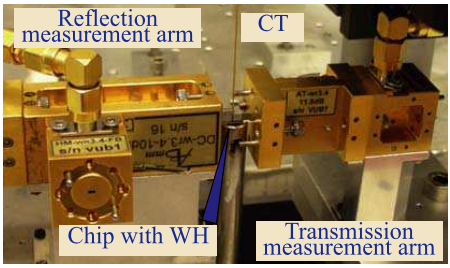

Figure 2. Measurement system: front end components of MVNA coupled to WH with an inserted CT.

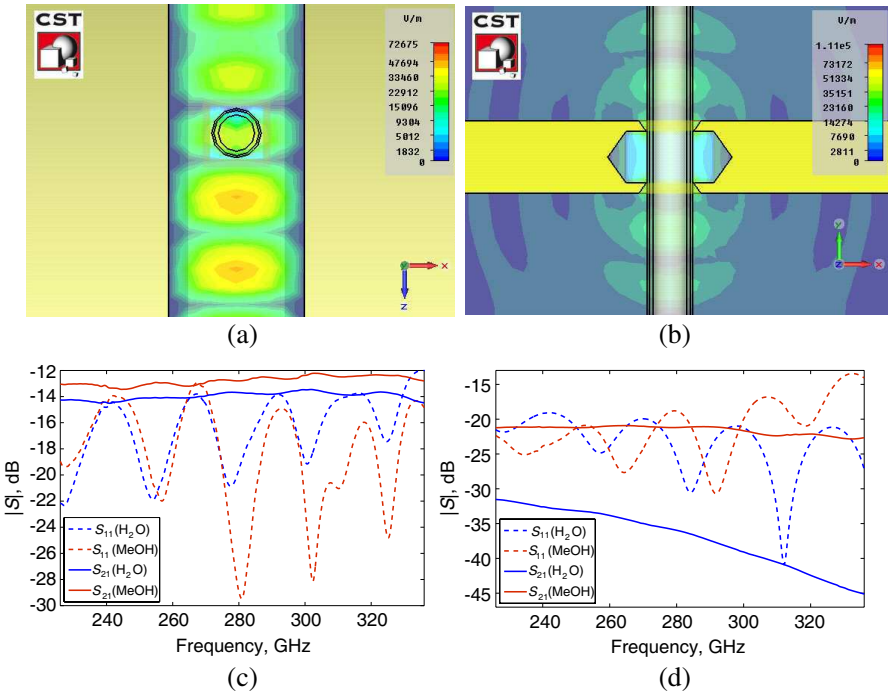

Figure 3. Simulation results. The absolute value of electric field (in V/m) distribution is plotted on (a) XZ- and (b) XY-planes. The color mapping is implemented in a logarithmic scale, while color bar labels are linear values. Frequency dependencies of reflection and transmission coefficients are shown for sensor configurations (c) WHCT100 and (d) WHCT320.

3. MODELING AND EXPERIMENTAL RESULTS

From 3D EM modeling and E-field distributions (see Figures 3(a), (b)) the conclusion can be drawn that the EM-wave propagating along the waveguide is partially reflected and partially transmitted through the CT and liquid contained in it (Figure 3(a)). The reflections of the EM wave occur at the WH-to-WR interfaces and on the CT itself. Hence standing waves exist between the WR-to-WH transition and the CT. Standing wave ratios, calculated from E-field distributions, indicate that for both WH-CT configurations the standing wave before the CT is larger than the one after the CT. Therefore the reflection at the CT is higher than at the WH-to-WR interface. This justifies that the simulated transmission and reflection spectra (Figures 3(c), (d))

featuring oscillatory frequency dependency and particularly the small oscillations of the transmission spectrum. The WR-to-WH impedance mismatch results from the fact that the WH has a slightly lower cut-off frequency. The WH was designed to be larger than the WR, in order to simplify the alignment task. Some of the EM energy is being radiated through the opening holes for the CT (Figure 3(b)).

The single mode waveguide concentrates the propagating THz wave on the part of CT inserted in the WH. The extent of the THz wave and liquid interaction is visible from the E-field intensity in the liquid Figures 3(a), (b). In WHCT100 a large amount of the E-field is concentrated in the shell of the CT and less in the liquid. In the case of WHCT320 more EM energy is concentrated in the liquid, and therefore more energy is absorbed. The absorption is related to the dielectric relaxation of the liquid. The transmitted EM-wave undergoes attenuation and phase shift specific to the CT material and liquid. It is desirable to have a low permittivity and absorption CT material (e.g., PTFE, PMMA), in order to reduce the reflection and absorption in the CT.

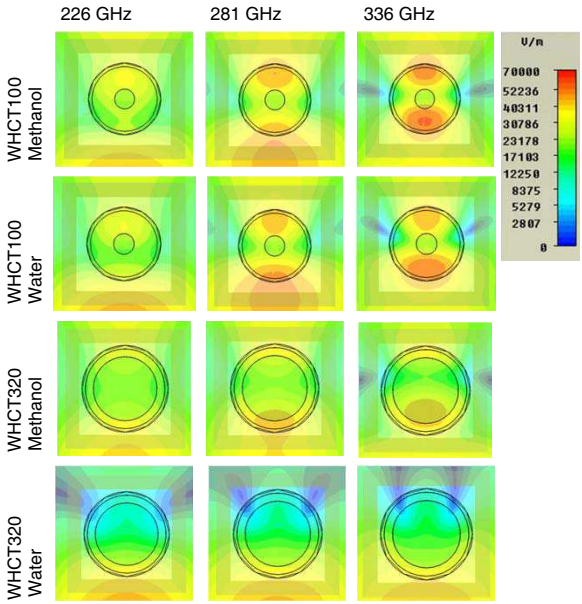

Figure 4. The THz wave E-field amplitude distribution on XZ-plane inside and around the CT. The results are plotted for the highest, lowest and middle frequencies of the band. The color mapping is implemented in a logarithmic scale, while color bar labels are linear values. The wave propagates from the bottom to the top.

In Figure 4 the XZ-plane E-field amplitude distributions are shown inside and around the CT of both WHCT100 and WHCT320 filled with water and methanol. Even if the small CT has a stronger local E-field when compared to a larger CT, the total amount of liquid molecules interacting with the EM wave is significantly larger. This increases the transmission signal response to the collective vibrational mode of molecules in the liquid. However, considering the WHCT320 E-field amplitude distribution in water, further increase in CT diameter would not bring additional sensitivity, because less power is being transmitted and more liquid is being shadowed.

The methanol was selected as a simple organic, well characterized, polar liquid for sensor demonstration purpose and comparison of different sensor configurations simulations and measurements. Furthermore the function of THz wave absorption versus methanol concentration should feature hydration curve by deviating from Beer-Lambert law. The averaged measured transmission amplitude S_{21} and corresponding $\pm 1\sigma$ error bars taken from five consecutive

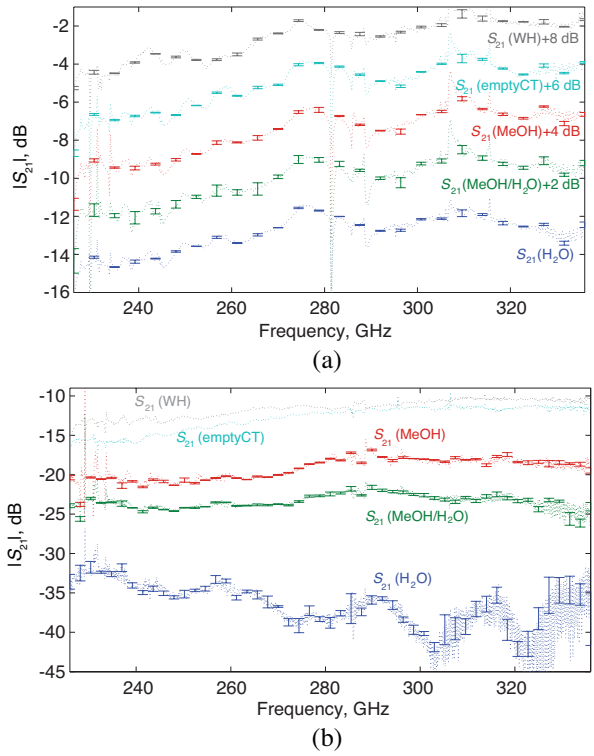

Figure 5. Transmission measurement results of (a) WHCT100 and (b) WHCT320 sensor configurations.

measurements are plotted in Figure 5 for the WHCT100 and WHCT320 configurations. In order to improve the visual quality of Figure 5(a), different offsets (expressed in dB) has been introduced for each curve. The measurements are performed with:

- S_{21} (WH) — empty WH;
- S_{21} (emptyCT) — WH and empty CT;
- S_{21} (MeOH) — WH-CT filled with pure methanol;
- S_{21} ($MeOH/H_2O$) — 50% methanol by volume mixture in deionized water;
- S_{21} (H_2O) — deionized water.

The reflection amplitude and phase of both transmission and reflection show no significant changes. The measurements (Figure 5) indicate that losses and distortions introduced by the CT (S_{21} (WH)-S_{21} (emptyCT)) are much smaller than for the CT filled with liquid (S_{21} (WH)-S_{21} (MeOH)), indicating that the transmitted EM-wave interaction is stronger with liquid. As expected, transmission for the WH-CT filled with water (S_{21} (H_2O)) is lower than with methanol (S_{21} (MeOH)). The absorption nonlinearity versus methanol concentration is demonstrated by the 50% methanol by volume mixture (S_{21} ($MeOH/H_2O$)). The measured transmission noise floor (−54 dB on average) is well below the measured signals in the major part of the band (226–325 GHz), but above 325 GHz the S_{21} (H_2O) level for WHCT320 is very close to the noise floor.

In order to evaluate the performance of the sensor, measurements on two well characterized liquids are performed. The difference between the transmission of WH-CT filled with methanol and water, S_{21} (MeOH)-S_{21} (H_2O), yields the water-to-methanol sensitivity of the sensor configuration. The higher the sensitivity the smaller the complex dielectric permittivity changes that can be detected, which is desirable for bio-sensing with THz. The simulated and measured water-to-methanol sensitivities of WHCT100 and WHCT320 are shown in Figure 6.

The water-to-methanol sensitivities, averaged over the frequency range, are 1.37 dB for WHCT100 and 17.55 dB for WHCT320. The highest water-to-methanol sensitivity of 26.69 dB is obtained for WHCT320 at 303 GHz. The liquid volumes enclosed in the WHCT100 and WHCT320 configurations are 4 nl and 40 nl, respectively. The sensor configuration with a CT of larger ID and thinner walls exhibits higher sensitivity, due to an increased EM wave interaction with the liquid. However, a CT with too large an internal diameter could result in excessive attenuation by the liquid, which might be inappropriate for a given measurement system.

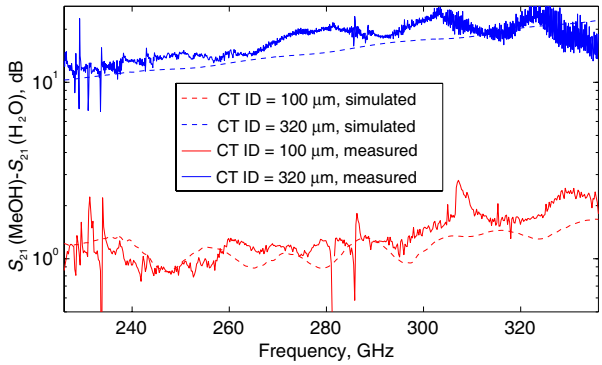

Figure 6. WHCT100 and WHCT320 sensor configurations' water-to-methanol sensitivities.

The simulated (see Figures 3(c), (d)) and measured (see Figure 5) transmission amplitude curves have different absolute values and shapes. The discrepancies in modeled and measured data might be caused by deviations of coupling losses, misalignment error and shape of the openings for CT from the modeled values. However, the average sensitivity difference and the frequency dependency are comparable for simulated and measured data. The misalignment error and WR-to-WH coupling parasitic reactance must be subtracted from the measurements by the introduction of flanges and the Thru-Reflect-Line de-embedding algorithm.

This method results in higher sensitivity than reported in [16], which is around 2 dB in 50–110 GHz. The sensitivity reported here can be further increased by applying resonant [22, 23] or differential techniques. The sensor configuration can also be used as a THz spectroscopy tool for liquids, utilizing numerical or analytical [24, 25] techniques to estimate the permittivity function of liquids in the CT. The dielectric parameter estimation can be achieved without waveguide calibration [26, 27] using CT with different IDs and same OD.

It is to be expected that biomolecules dissolved in water perturb the water's hydrogen bonding network dynamics in their vicinity, creating in this way a hydration shell of more tightly (or loosely) bound and thus slower (or faster) water molecules. As the dipolar relaxation time constant of water molecules in the hydration shell is different from that in bulk water, the hydration shell absorption will be lower or higher compared to bulk water depending on whether the biomolecule is chemotropic (slower water molecules in the hydration shell) or chaotropic (faster water molecules in the hydration shell).

Collective protein-water network dynamics probed by THz

Table 1. HSA complex refractive index [28], simulated WHCT320 transmission and sensitivities.

HSA	Natural	Unfolded	Natural	Unfolded
Frequency, GHz	250	250	300	300
n	2.66	2.80	2.48	2.65
α, cm^{-1}	117	109	123	116
$\lvert S_{21}^S \rvert$, dB	−17.32	−17.01	−32.27	−30.48
Sensitivity, dB	0.31		1.79	

spectroscopy for native, extended and unfolded human serum albumin (HSA) conformations proves that the HSA hydration layer is dependent on its conformation [28]. This indicates that the surface area, number of exposed hydrophobic or hydrophilic functional groups, and volume of the molecule are correlated with the biomolecules' hydration shell. Hence, changes occurring on the biomolecular level through changes in the hydration layer of biomolecules give rise to changes in THz response.

The transmission spectrum of a WHCT sensor configuration is strongly influenced by the liquids' absorption of THz waves. Therefore the WHCT sensor enables the detection of biomolecule hydration layer changes. To estimate if the WHCT can detect the dielectric permittivity changes occurring during HSA thermal denaturing, the dielectric parameters were taken from [28] and simulated with our WHCT320 model. The parameters and simulation results for a 1 mM HSA mixture are summarized in Table 1.

4. CONCLUSION

The presented sensor configuration uses THz radiation to probe changes occurring at the biomolecular level in liquids and highly hydrated specimens. THz spectroscopy of liquids was previously hindered by low sensitivities in comparison to other measurement techniques. The sensitivity is increased by utilizing low-loss integrated waveguides and improving the interaction strength between the THz-wave and the liquid. The interaction level is controlled by changing the liquid volume enclosed in the waveguide. The unprecedented water-to-methanol sensitivity (average — 17.55 dB, maximal — 26.69 dB) in a 226–336 GHz frequency range is achieved using room temperature operated solid state source and detectors. An estimated sensitivity value of 1.8 dB of this first sensor prototype to conformational changes in human serum albumin reveals the THz biosensing potential of this

method. A capillary tube is an appealing vessel for THz spectroscopy tool due to its common usage in life sciences and disposability.

ACKNOWLEDGMENT

The first author is thankful to IMEC (Leuven, Belgium) for its scholarship program. The work was partially executed in the framework of ESF-RPN, NEWFOCUS program. The first author is grateful for the help received from Pavel Poliakov (IMEC, Leuven) and Sergej Deutsch (Cadence Design Systems).

REFERENCES

1. Leitner, D. M., M. Gruebele, and M. Havenith, "Solvation dynamics of biomolecules: Modeling and terahertz experiments," *HFSP J.*, Vol. 2, 314–323, Dec. 2008.
2. Born, B., S. J. Kim, S. Ebbinghaus, M. Gruebele, and M. Havenith, "The terahertz dance of water with the proteins: The effect of protein flexibility on the dynamical hydration shell of ubiquitin," *Faraday Discuss.*, Vol. 141, 161–173, 2009.
3. Heyden, M., J. Sun, S. Funkner, G. Mathias, H. Forbert, M. Havenith, and D. Marx, "Dissecting the THz spectrum of liquid water from first principles via correlations in time and space," *Proc. Natl. Acad. Sci. USA*, Vol. 107, 12068–12073, Jul. 2010.
4. Tielrooij, K. J., D. Paparo, L. Piatkowski, H. J. Bakker, and M. Bonn, "Dielectric relaxation dynamics of water in model membranes probed by terahertz spectroscopy," *Biophys. J.*, Vol. 97, 2484–2492, Nov. 2009.
5. Hishida, M. and K. Tanaka, "Long-range hydration effect of lipid membrane studied by terahertz time-domain spectroscopy," *Phys. Rev. Lett.*, Vol. 106, 158102, Apr. 2011.
6. Brucherseifer, M., M. Nagel, P. Bolivar, H. Kurz, A. Bosserhoff, and R. Buttner, "Label-free probing of the binding state of dna by time-domain terahertz sensing," *Appl. Phys. Lett.*, Vol. 77, 4049–4051, Dec. 2000.
7. Markelz, A., S. Whitmire, J. Hillebrecht, and R. Birge, "THz time domain spectroscopy of biomolecular conformational modes," *Phys. Med. Biol.*, Vol. 47, 3797–3805, Nov. 2002.
8. Liu, R., M. He, R. Su, Y. Yu, W. Qi, and Z. He, "Insulin amyloid fibrillation studied by terahertz spectroscopy and other biophysical methods," *Biochem. Biophys. Res. Commun.*, Vol. 391, 862–867, Jan. 2010.

9. Markelz, A. G., "Terahertz dielectric sensitivity to biomolecular structure and function," *IEEE J. Sel. Top. Quant.*, Vol. 14, 180–190, Jan.–Feb. 2008.
10. Markelz, A., A. Roitberg, and E. Heilweil, "Pulsed terahertz spectroscopy of dna, bovine serum albumin and collagen between 0.1 and 2.0 THz," *Chem. Phys. Lett.*, Vol. 320, 42–48, Mar. 2000.
11. Chen, J.-Y., J. R. Knab, J. Cerne, and A. G. Markelz, "Large oxidation dependence observed in terahertz dielectric response for cytochrome c," *Phys. Rev. E*, Vol. 72, 040901, Oct. 2005.
12. Knab, J., J.-Y. Chen, and A. Markelz, "Hydration dependence of conformational dielectric relaxation of lysozyme," *Biophys. J.*, Vol. 90, No. 7, 2576–2581, 2006.
13. Bolivar, P., M. Brucherseifer, M. Nagel, H. Kurz, A. Bosserhoff, and R. Buttner, "Label-free probing of genes by time-domain terahertz sensing," *Phys. Med. Biol.*, Vol. 47, 3815–3821, Nov. 2002.
14. Bolivar, P., M. Nagel, F. Richter, M. Brucherseifer, H. Kurz, A. Bosserhoff, and R. Buttner, "Label-free THz sensing of genetic sequences: Towards 'THz biochips'," *Philos. T. Roy. Soc. A*, Vol. 362, 323–333, Feb. 2004.
15. Kasai, S., A. Tanabashi, K. Kajiki, T. Itsuji, R. Kurosaka, H. Yoneyama, M. Yamashita, H. Ito, and T. Ouchi, "Micro strip line-based on-chip terahertz integrated devices for high sensitivity biosensors," *Appl. Phys. Express*, Vol. 2, Jun. 2009.
16. Laurette, S., A. Treizebre, F. Affouard, and B. Bocquet, "Subterahertz characterization of ethanol hydration layers by microfluidic system," *Appl. Phys. Lett.*, Vol. 97, Sep. 2010.
17. Hasar, U. C., "Microwave method for thickness-independent permittivity extraction of low-loss dielectric materials from transmission measurements," *Progress In Electromagnetics Research*, Vol. 110, 453–467, 2010.
18. Hasar, U. C., "Unique permittivity determination of low-loss dielectric materials from transmission measurements at microwave frequencies," *Progress In Electromagnetics Research*, Vol. 107, 31–46, 2010.
19. Barroso, J. J., and A. L. de Paula, "Retrieval of permittivity and permeability of homogeneous materials from scattering parameters," *Journal of Electromagnetic Waves and Applications*, Vol. 24, No. 11–12, 1563–1574, 2010.
20. Matvejev, V., C. de Tandt, W. Ranson, and J. Stiens, "Wet silicon bulk micromachined THz waveguides for low-loss integrated

sensor applications," *2010 IEEE 35th International Conference on Infrared, Millimeter, and Terahertz Waves (IRMMW-THz 2010)*, 2, Piscataway, NJ, USA, 2010.

21. Barthel, J., K. Bachhuber, R. Buchner, and H. Hetzenauer, "Dielectric spectra of some common solvents in the microwave region — water and lower alcohols," *Chem. Phys. Lett.*, Vol. 165, 369–373, Jan. 1990.
22. Li, E., Z.-P. Nie, G. Guo, Q. Zhang, Z. Li, and F. He, "Broadband measurements of dielectric properties of low-loss materials at high temperatures using circular cavity method," *Progress In Electromagnetics Research*, Vol. 92, 103–120, 2009.
23. Addamo, G., G. Virone, D. Vaccaneo, R. Tascone, O. A. Peverini, and R. Orta, "An adaptive cavity setup for accurate measurements of complex dielectric permittivity," *Progress In Electromagnetics Research*, Vol. 105, 141–155, 2010.
24. Nishikata, A., "Scattering analysis for layered cylindrical object perpendicularly piercing the wider walls of a rectangular waveguide and its application to epsilon(r) and mu(r) measurement," *IEEE T. Microw. Theory*, Vol. 57, 1602–1611, Jun. 2009.
25. Bucinskas, J., L. Nickelson, and V. Sugurovas, "Microwave diffraction characteristic analysis of 2D multilayered uniaxial anisotropic cylinder," *Progress In Electromagnetics Research*, Vol. 109, 175–190, 2010.
26. Hasar, U. C., O. Simsek, M. K. Zateroglu, and A. E. Ekinci, "A microwave method for unique and non-ambiguous permittivity determination of liquid materials from measured uncalibrated scattering parameters," *Progress In Electromagnetics Research*, Vol. 95, 73–85, 2009.
27. Kadiroglu, F. and U. C. Hasar, "A highly accurate microwave method for permittivity determination using corrected scattering parameter measurements," *Journal of Electromagnetic Waves and Applications*, Vol. 24, No. 16, 2179–2189, 2010.
28. Luong, T. Q., P. K. Verma, R. K. Mitra, and M. Havenith, "Do hydration dynamics follow the structural perturbation during thermal denaturation of a protein: A terahertz absorption study," *Biophys. J.*, Vol. 101, 925–933, Aug. 17, 2011.